Developmental Biology 393 (2014) 10–23

Contents lists available at ScienceDirect

Developmental Biology

journal homepage: www.elsevier.com/locate/developmentalbiology

Resource

Visualizing the cell-cycle progression of endothelial cells in zebrafish

Shigetomo Fukuhara [a,*], Jianghui Zhang [a], Shinya Yuge [a], Koji Ando [a], Yuki Wakayama [a], Asako Sakaue-Sawano [b,c], Atsushi Miyawaki [b,c], Naoki Mochizuki [a,d,*]

[a] Department of Cell Biology, National Cerebral and Cardiovascular Center Research Institute, Fujishirodai 5-7-1, Suita, Osaka 565-8565, Japan
[b] Laboratory for Cell Function and Dynamics, Advanced Technology Development Group, Brain Science Institute, RIKEN, 2-1 Hirosawa, Wako City, Saitama 351-0198, Japan
[c] Life Function and Dynamics, ERATO, JST, 2-1 Hirosawa, Wako City, Saitama 351-0198, Japan
[d] JST-CREST, Tokyo, Japan

ARTICLE INFO

Article history:
Received 20 March 2013
Received in revised form
6 June 2014
Accepted 18 June 2014
Available online 26 June 2014

Keywords:
Endothelial cell
Cell cycle
Vascular development
Angiogenesis
Proliferation

ABSTRACT

The formation of vascular structures requires precisely controlled proliferation of endothelial cells (ECs), which occurs through strict regulation of the cell cycle. However, the mechanism by which EC proliferation is coordinated during vascular formation remains largely unknown, since a method of analyzing cell-cycle progression of ECs in living animals has been lacking. Thus, we devised a novel system allowing the cell-cycle progression of ECs to be visualized in vivo. To achieve this aim, we generated a transgenic zebrafish line that expresses zFucci (zebrafish fluorescent ubiquitination-based cell cycle indicator) specifically in ECs (an EC-zFucci Tg line). We first assessed whether this system works by labeling the S phase ECs with EdU, then performing time-lapse imaging analyses and, finally, examining the effects of cell-cycle inhibitors. Employing the EC-zFucci Tg line, we analyzed the cell-cycle progression of ECs during vascular development in different regions and at different time points and found that ECs proliferate actively in the developing vasculature. The proliferation of ECs also contributes to the elongation of newly formed blood vessels. While ECs divide during elongation in intersegmental vessels, ECs proliferate in the primordial hindbrain channel to serve as an EC reservoir and migrate into basilar and central arteries, thereby contributing to new blood vessel formation. Furthermore, while EC proliferation is not essential for the formation of the basic framework structures of intersegmental and caudal vessels, it appears to be required for full maturation of these vessels. In addition, venous ECs mainly proliferate in the late stage of vascular development, whereas arterial ECs become quiescent at this stage. Thus, we anticipate that the EC-zFucci Tg line can serve as a tool for detailed studies of the proliferation of ECs in various forms of vascular development in vivo.

Introduction

The vasculature is the earliest organ to form in the developing vertebrate embryo. The formation of blood vessels occurs through two fundamentally distinct processes, vasculogenesis and angiogenesis (Carmeliet, 2000; Risau, 1997; Risau and Flamme, 1995). Vasculogenesis constitutes the *de novo* formation of a primitive vascular network through the differentiation of mesodermal cells into vascular precursor cells (angioblasts) and their subsequent proliferation, coalescence, and remodeling. On the other hand, angiogenesis is the process of new blood vessel formation which involves sprouting of ECs (ECs) from preexisting vessels, followed by their proliferation and migration. Precise control of the proliferation of ECs is essential for both vasculogenesis and angiogenesis (Ausprunk and Folkman, 1977; Herbert and Stainier, 2011). Although several studies have investigated the mechanisms governing EC proliferation, the dynamics of this proliferation during vascular development in vivo remain poorly understood.

Cell proliferation is strictly regulated by the cell cycle, which is divided into four phases: G1 (first gap), S (DNA synthesis), G2 (second gap), and M (mitosis). The cell-cycle control of ECs has long been studied using in vitro models in which cultured ECs are plated on plastic dishes (Akimoto et al., 2000; Favot et al., 2004; Kimura et al., 2000; Zhou et al., 2012). However, little is known about how the cell cycle of ECs is coordinated during vascular development, since a method allowing the cell-cycle progression of ECs to be analyzed in living animals has not been available. To date, 5-bromo-2′-deoxyuridine (BrdU) or 5-ethynyl-2′-deoxyuridine (EdU) labeling has been utilized to detect S phase cells in tissue samples (Yu et al., 1992). Besides BrdU or EdU labeling, cell proliferation in tissue

* Corresponding authors: Department of Cell Biology, National Cerebral and Cardiovascular Center Research Institute, 5-7-1 Fujishirodai, Suita, Osaka 565-8565, Japan. Fax: +81 6 6835 5461.
E-mail addresses: fuku@ncvc.go.jp (S. Fukuhara), nmochizu@ri.ncvc.go.jp (N. Mochizuki).

http://dx.doi.org/10.1016/j.ydbio.2014.06.015
0012-1606/

samples can also be assessed by immunohistochemistry with antibodies against cell-cycle and proliferation markers such as proliferating cell nuclear antigen, phosphohistone-H3 and Ki-67 (Cattoretti et al., 1992; Hendzel et al., 1997; Yu et al., 1992). However, these techniques do not allow assessment of cell-cycle progression and cell proliferation in living animals. To overcome this problem, Tg zebrafish lines with ECs expressing fluorescent proteins tagged with a nuclear localization signal (NLS) were established (Roman et al., 2002). Although these Tg lines enable ECs undergoing mitosis to be observed, they cannot be used to analyze the cell-cycle progression dynamics of ECs.

Cell-cycle progression is mediated by the levels of cell-cycle regulators, which are strictly controlled by the ubiquitination-dependent protein degradation pathway throughout the cell cycle (Ang and Harper, 2004; Nakayama and Nakayama, 2006). By harnessing the regulation of cell-cycle dependent ubiquitination, we developed a genetically encoded biosensor for cell-cycle progression: Fucci (fluorescent ubiquitination-based cell cycle indicator) (Sakaue-Sawano et al., 2008). Fucci is a set of fluorescent probes, which are generated by fusing red and green fluorescent proteins to the ubiquitination domains of human Cdt1 and human geminin, respectively. In the cells expressing these probes, the nuclei of G0/G1 phase cells and those of S/G2/M phase cells can be identified by red and green fluorescence, respectively. In addition, we also generated a Fucci derivative (zFucci) allowing visualization of cell-cycle progression in zebrafish (Sugiyama et al., 2009). Since zebrafish embryos are transparent, transgenic fish embryos expressing zFucci probes provide a powerful tool for visualizing cell-cycle dynamics in living animals.

In the present study, we succeeded in developing an EC-specific zFucci transgenic (EC-zFucci Tg) line, thereby allowing the cell-cycle dynamics of ECs to be visualized in vivo. Exploiting this line, we visualized the cell-cycle progression of ECs during the development of several types of vascular structures including intersegmental vessels (ISVs), caudal vessels, and hindbrain vessels. We also studied the late stage of vascular development. Our analyses clearly show the advantages of using the EC-zFucci Tg line for studying EC proliferation in vivo.

Materials and methods

Plasmid construction

The Tol2 vector system was kindly provided by K. Kawakami (National Institute of Genetics, Japan) (Kawakami et al., 2004; Urasaki et al., 2006). The pTolfli1 vector was constructed by removing a cDNA fragment containing green fluorescence protein (GFP) and Gateway cassette from the pTolfli1epEGFPDest plasmid, a gift from N. Lawson (University of Massachusetts Medical School) (Lawson and Weinstein, 2002). To generate the pTolflk1 plasmid, the *fli1* enhancer/promoter was removed from the pTolfli1 vector, and replaced with the *flk1* promoter, a gift from D.Y. Stainier (The University of California, San Francisco) (Jin et al., 2005b).

The S/G2/M marker for fish cells was generated by fusing monomeric (m)Venus to the N-terminal 100 aa of zebrafish geminin (mV-zGem), while the G0/G1 marker was composed of mCherry and the N-terminal 190 aa of zebrafish Cdt1 (mC-zCdt) (Sugiyama et al., 2009). To construct the pTolflk1-mVenus-zGem (1/100) and pTol1flk1-mCherry-zCdt1 (1/190), cDNA fragments encoding mV-zGem and mC-zCdt were subcloned into the pTolflk1 vector, respectively, as shown in Fig. 1A. An oligonucleotide encoding NLS derived from SV40 (PKKKRKV) was inserted into the EcoRI/XhoI sites of a pcDNA3-td-EosFP vector (Molecular Biotechnology) to generate the plasmid encoding NLS-tagged tandem dimer Eos fluorescence protein (NLS-Eos). To construct the pTolflk1-NLS-Eos vector, NLS-Eos cDNA was subcloned into the pTolflk1 vector. Similarly, a cDNA expressing NLS-tagged mCherry was subcloned into the pTolflk1 vector to yield pTolflk1-NLS-mCherry. An oligonucleotide encoding the myristoylation (Myr) signal derived from Lyn kinase was subcloned into pEGFP-N1 and pmCherry-N1 vectors (Clontech, Takara Bio Inc.) to construct the plasmid encoding Myr signal-tagged GFP (Myr-GFP) and that encoding Myr signal-tagged mCherry (Myr-mCherry), respectively. The pTolfli1-Myr-GFP and pTolfli1-Myr-mCherry were constructed by inserting Myr-GFP and Myr-mCherry cDNA into the pTolfli1 vector, respectively. Details can be provided upon request.

Zebrafish husbandry

Zebrafish were maintained and bred under standard conditions. Embryos were staged by hours post-fertilization (hpf) at 28 °C (Kimmel et al., 1995). Animal experiments were approved by the animal committee of the National Cerebral and Cardiovascular Center and performed according to the regulations of the National Cerebral and Cardiovascular Center.

Generation of transgenic zebrafish lines

Tol2 transposase mRNA was in vitro transcribed with SP6 RNA polymerase, using NotI-linearized pCS-TP vector as a template, employing the mMESSAGE mMACHINE kit (Ambion) (Kawakami et al., 2004; Urasaki et al., 2006). To generate the *Tg(flk1:mV-Gem)*, *Tg(flk1:mC-Cdt)*, *Tg(flk1:NLS-mCherry(mC))*, *Tg(flk1:NLS-Eos)*, *Tg(fli1:Myr-GFP)* and *Tg(fli1:Myr-mCherry(mC))* fish lines, the Tol2 plasmids constructed as described above were microinjected along with Tol2 transposase RNA into one-cell stage embryos to generate transgenic lines. Embryos showing transient expression of fluorescence proteins in the vasculature were selected, raised to adulthood, and became founders in which germline transmission was confirmed.

in vivo imaging

Embryos were dechorionated and anesthetized in 0.016% tricaine (Sigma-Aldrich) in E3 embryo medium (5 mM NaCl, 0.17 mM KCl, 0.33 mM $CaCl_2$, 0.33 mM $MgSO_4$). The embryos were mounted in 1% low-melting agarose dissolved in E3 medium poured on a 35-mm-in-diameter glass-base dish (Asahi Techno Glass), and submerged in E3 medium supplemented with 0.016% tricaine and 0.2 mM phenylthiourea. Confocal images were taken with an FV1000 (Olympus) confocal upright microscope system equipped with water-immersion 10× (LUMPlanFL, NA 0.30), 20× (XLUMPlanFL, NA 1.0) and 40× (LUMPlanFL, NA 0.80) lenses. The 473 nm and 559 nm laser lines were employed for green-yellow fluorescent proteins (mVenus and Eos) and red fluorescent proteins (mCherry and photoconverted Eos), respectively. For confocal time-lapse imaging, images were collected every 10–15 min for 5–10 h. To avoid cross-detection of green and red signals, images were acquired sequentially at 473 nm and 559 nm. Image files were processed and analyzed using Volocity software (Improvision).

Whole-mount immunohistochemistry and EdU labeling

For whole-mount immunohistochemistry, embryos were fixed in 4% paraformaldehyde (PFA) in phosphate buffered saline (PBS) at 4 °C overnight, washed with PBS, dehydrated in 100% MeOH at −20 °C overnight, and rehydrated by serial incubations with PBS and MeOH (75% MeOH/25% PBS for 5 min, 50% MeOH/50% PBS for 5 min, 25% MeOH/75% PBS for 5 min, 100% PBS for 5 min). The embryos were then permeabilized in PBS containing 0.1% Tween 20 and 0.1% Triton X-100 (PBSTX) four times for 5 min, and blocked with PBSTX containing 1% bovine serum albumin and

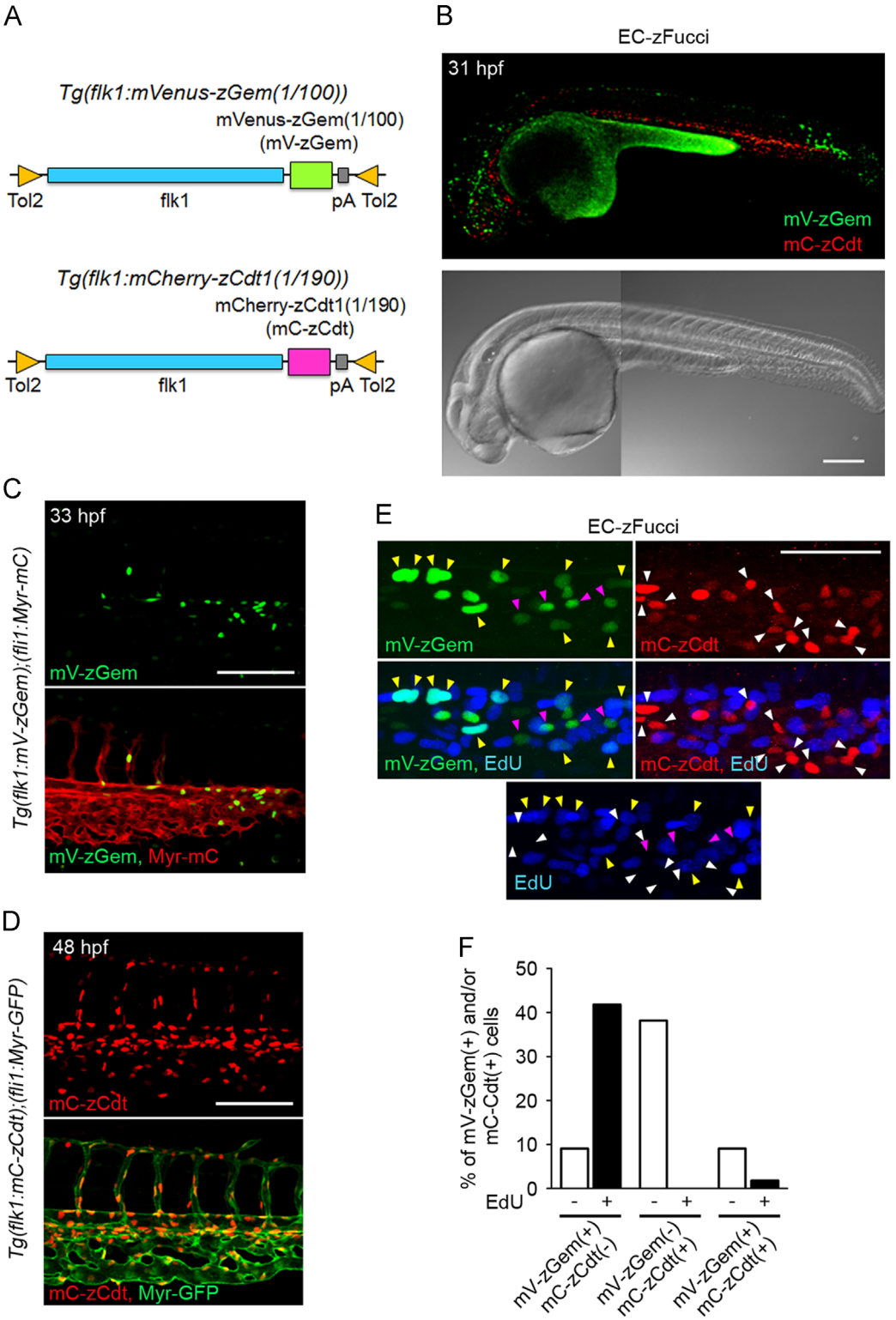

Fig. 1. Development and characterization of transgenic zebrafish lines expressing zFucci cell-cycle biosensors in endothelial cells (ECs). (A) Schematic representation of the plasmids used for delivering transgenes expressing mVenus-zGem (1/100) (mV-zGem) and mCherry-zCdt1(1/190) (mC-zCdt) under control of the *flk1* promoter. (B) Upper, fluorescence image (mV-zGem [green] and mC-zCdt1 [red]) of an EC-zFucci, *Tg(flk1:mV-zGem);(flk1:mC-Cdt)* embryo, at 31 hpf; lower, bright field images. (C) 3D-rendered confocal stack fluorescence images of the caudal regions of the *Tg(flk1:mV-zGem);(fli1:Myr-mC)* embryo at 33 hpf. Upper, mVenus image; lower, the merged image of mVenus (green) and mCherry (red). All of the confocal fluorescence images are lateral views and displayed as anterior to the left, unless otherwise described, in the following images. (D) 3D-rendered confocal images of the caudal regions of the *Tg(flk1:mC-Cdt);(fli1:Myr-GFP)* embryo at 48 hpf. Upper, mCherry image; lower, the merged image of mVenus (green) and mCherry (red). (E) Images of the EC-zFucci embryo at 29.5 hpf treated with EdU for 1 h. mVenus images (green), mCherry images (red) and EdU images visualized by Alexa 647-azide (blue) of the trunk vessel are shown as indicated at the lower left corner of the image. Yellow, pink and white arrowheads indicate mV-zGem/EdU double-positive cells, mV-zGem-positive/EdU-negative cells and mC-zCdt-positive/EdU-negative cells, respectively. (F) Percentages of mV-zGem-positive, mC-zCdt-positive and mV-zGem/mC-zCdt double positive cells labeled without (−) or with (+) EdU as observed in E were quantified (n=55). Scale bars, 200 μm (B) and 100 μm (C–E).

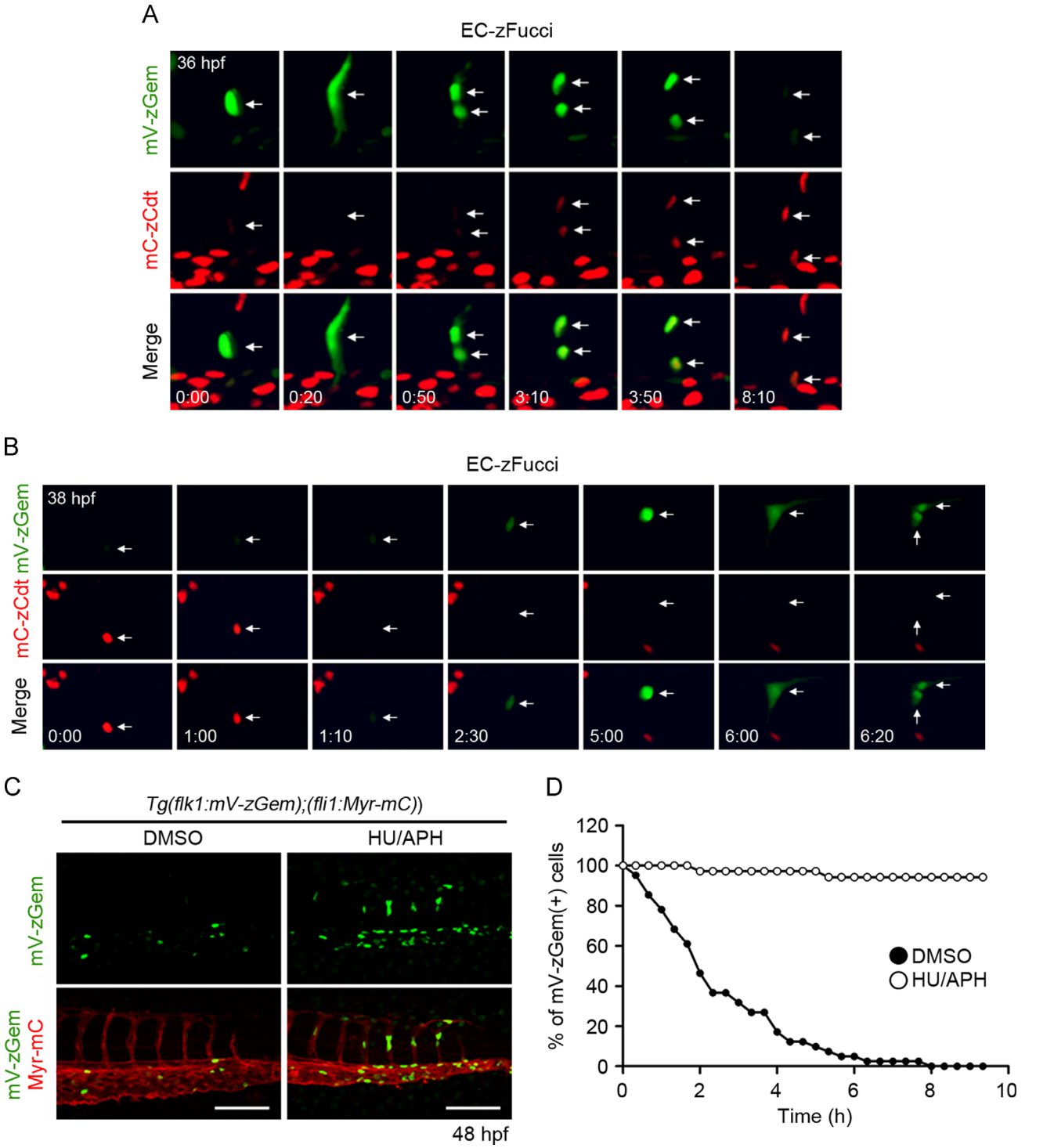

Fig. 2. Validation of the EC-zFucci Tg fish line. (A) Confocal 3D fluorescence image of the intersegmental vessel (ISV) of an EC-zFucci embryo at 36 hpf (first column) and the corresponding subsequent time-lapse images (from second to sixth columns) at the elapsed time (h:min) indicated at the bottom. Top, mVenus images; middle, mCherry images; bottom, the merged images. Note that an mV-zGem-positive cell (arrows at 0:00 and 0:20) divides into two daughter cells (arrows at 0:50), which subsequently lose mVenus fluorescence and start to emit mCherry fluorescence (arrows at 3:10, 3:50 and 8:10). (B) Confocal 3D fluorescence image of the ISV of an EC-zFucci embryo at 38 hpf (first column) and the corresponding subsequent time-lapse images (from second to seventh columns) at the elapsed time (h:min) indicated at the bottom are shown, essentially as in A. Note that the mC-zCdt-positive cell (arrows at 0:00 and 1:00) loses mCherry fluorescence (arrow at 1:10), starts to emit mVenus fluorescence (arrows at 2:30, 5:00 and 6:00), and subsequently divides into two daughter cells (arrows at 6:20 and 7:00). (C) 3D-rendered confocal images of the caudal regions of 48 hpf *Tg(flk1:mV-zGem);(fli1:Myr-mC)* embryos treated with either DMSO or both hydroxyurea and aphidicolin (HU/APH) from 30 to 48 hpf. Upper, mVenus images; lower, the merged images of mVenus and mCherry. Scale bars, 100 μm. (D) Duration: time that mVenus-positive cells in the EC-zFucci Tg embryos at 36 hpf continue to emit mVenus fluorescence. *Tg (flk1:mV-zGem);(fli1:Myr-mC)* embryos were treated from 30 hpf with either DMSO (closed circles) or HU/APH (open circles), and time-lapse imaged starting at 36 hpf for 9 h 20 min to track the mVenus-positive cells. The *y*-axis indicates the number of mVenus-positive cells, while the *x*-axis shows the time after starting the time-lapse imaging. Data are expressed as percentages relative to that observed at the beginning of the imaging (DMSO [$n=35$], HU/APH [$n=41$]).

0.1% normal goat serum for 2 h at room temperature (RT). Then, the embryos were stained with anti-GFP mouse monoclonal antibody (Clontech, Takara Bio Inc.) and anti-DsRed rabbit polyclonal antibody (Clontech, Takara Bio Inc.) at 4 °C overnight to detect mVenus and mCherry, respectively. Proteins reacting with the primary antibody were visualized with species-matched Alexa

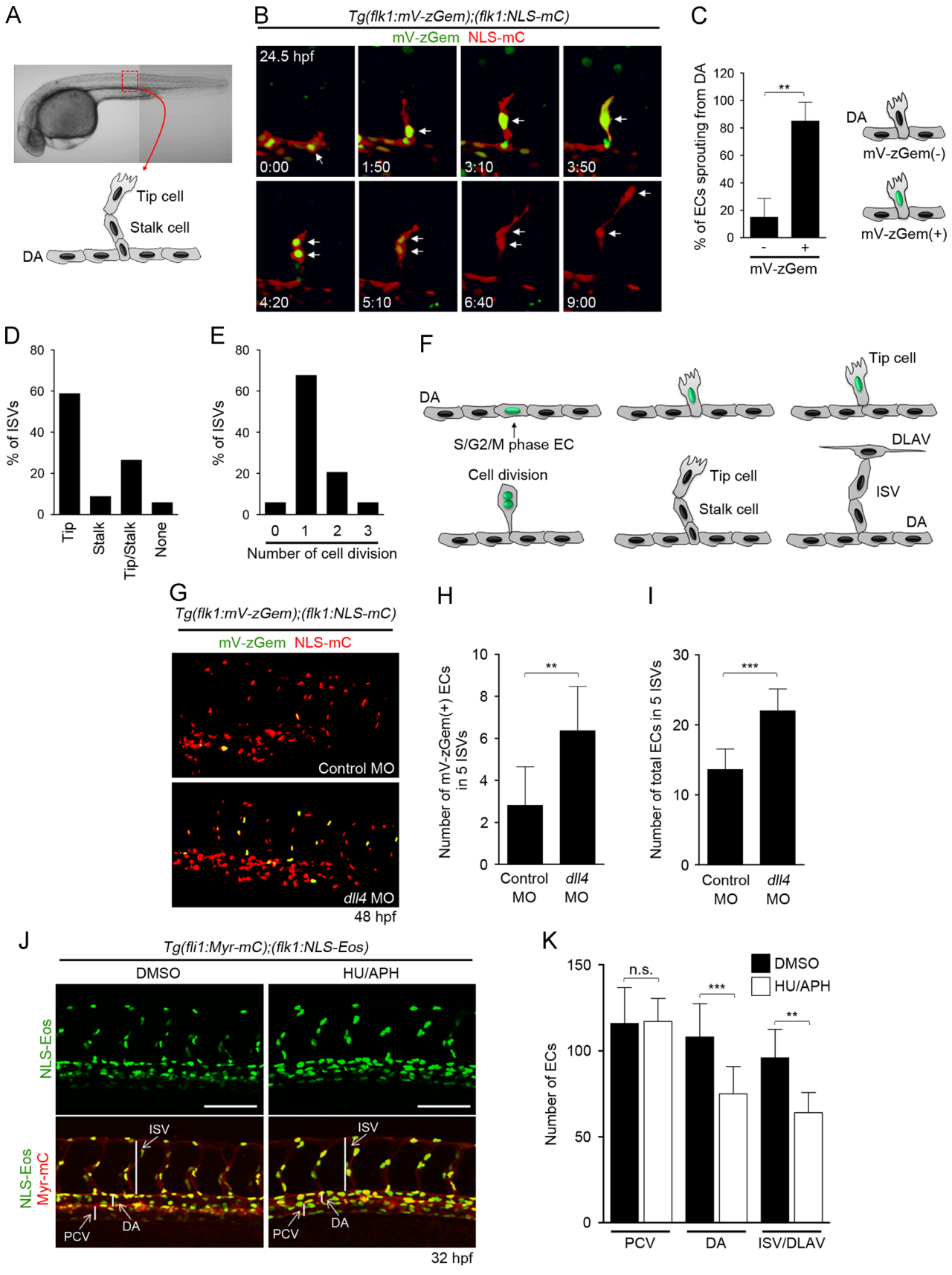

488- and Alexa 546-labeled secondary antibodies (Molecular Probes, Invitrogen).

EdU labeling was performed using the Click-iT EdU Alexa Flour imaging kit (Molecular Probes, Invitrogen) basically according to the manufacturer's instructions. *Tg(flk1:mV-zGem);Tg(flk1:mC-zCdt)* fish embryos were dechorionated at 28.5 hpf, and incubated with 400 μM EdU for 1 h at 28 °C. After fixation and permeabilization, the embryos were rinsed with ddH_2O, then incubated with Alexa 647-azaide for 30 min at RT, and finally subjected to whole-mount immunohistochemistry as described above.

Fluorescence images of Alexa 488, Alexa 546 and Alexa 647 were recorded with an FV1000 confocal upright microscope system equipped with 473 nm, 559 nm and 633 nm laser lines, respectively.

Morpholino oligonucleotide (MO) injections

For morpholino oligonucleotide (MO)-mediated gene knockdown, embryos were injected at the one-cell or two-cell stage with control MO (Gene Tools), 5 ng of *delta-like 4* (*dll4)* MO, and 5 ng of *ckdn1b cyclin-dependent kinase inhibitor 1B* (*cdkn1b)* MO (Gene Tools). The sequences for the already-validated MOs used in this study are *dll4* MO, 5′-TAGGGTTTAGTCTTACCTTGGTCAC-3′ (Siekmann and Lawson, 2007); *ckdn1b* MO, 5′-ACGGTCAAAATT-CAAAGCACATACC-3′ (Nicoli et al., 2012).

Photoconversion

Tg(flk1:NLS-Eos) fish embryos were dechorionated at the stage indicated in the figure legend, and mounted as described above. The NLS-Eos-positive ECs at the growing edges of caudal vessels were photolabelled by photoconverting the fluorescence of NLS-Eos from green to red. For photoconversion, a 405 nm laser was focused onto an area of interest for 60 s × 2 with 100% power, 10 μs/pixel (tornado function). The embryos were then subjected to time-lapse imaging as described above.

Chemical treatment

To block the cell cycle, embryos were treated with 150 μM aphidicolin (APH) and 20 mM hydroxyurea (HU) in the E3 embryo medium containing 4% dimethyl sulfoxide (DMSO) as described previously (Zhang et al., 2008).

Statistical analysis

Data were analyzed using GraphPad Prism software (GraphPad Software Inc.). Statistical significance was determined using a two-tailed Mann–Whitney U test for paired samples or one-way analysis of variance and nonparametric tests for multiple groups. *P*-values < 0.05 were considered statistically significant.

Results

Development of a transgenic zebrafish line expressing cell-cycle biosensor zFucci specifically in ECs

To visualize the cell-cycle progression of ECs in living animals, we developed a transgenic zebrafish line that expresses either a S/G2/M marker, mVenus-zGeminin(1/100) (mV-zGem), or a G0/G1 marker, mCherry-zCdt1(1/190) (mC-zCdt), under *flk1* promoter control (Fig. 1A). We crossbred these fish to generate a double Tg zebrafish line, *Tg(flk1:mV-zGem);(flk1:mC-zCdt)*, which we call EC-specific zFucci (EC-zFucci) Tg fish (Fig. 1B). To confirm EC-specific expressions of mV-zGem and mC-zCdt in the EC-zFucci fish, we analyzed two double Tg embryos, *Tg(flk1:mV-zGem);(fli1:Myr-mC)* and *Tg(flk1:mC-zCdt);(fli1:Myr-GFP)*. In the *Tg(flk1:mV-zGem);(fli1:Myr-mC)* fish embryo, mV-zGem expression was confined to mCherry fluorescence-marked ECs (Fig. 1C). Similarly, mCherry fluorescence was detected in the nuclei of GFP fluorescence-marked ECs in the *Tg(flk1:mC-zCdt);(fli1:Myr-GFP)* fish embryo (Fig. 1D). These findings indicate that the EC-zFucci fish line exhibits EC-specific expressions of mV-zGem and mC-zCdt. However, the fluorescence signals of mV-zGem and mC-zCdt were only weakly detected in the axial vessels of the EC-zFucci fish embryo before 24 hpf. Therefore, the EC-zFucci reporter line may not be suitable for analyzing the cell-cycle dynamics of ECs during the early stage of vascular development.

Next, we confirmed that mVenus and mCherry fluorescence in the EC-zFucci embryos actually mark ECs in the S/G2/M and G1 phases of the cell cycle, respectively. First, we pulse-labeled an EC-zFucci fish with EdU at 29.5 hpf for 1 h to identify S-phase cells. In the trunk regions, most of the mVenus-positive cells were labeled with EdU, whereas none of the mCherry-positive cells showed EdU incorporation, indicating that ECs in the S phase are marked selectively by mVenus fluorescence in the EC-zFucci embryos (Fig. 1E, F). In addition, we tracked either mCherry or mVenus fluorescence-positive ECs in the EC-zFucci embryo by performing time-lapse imaging. We observed the mVenus-positive EC to divide into two daughter cells, which subsequently lost mVenus fluorescence and started to exhibit mCherry fluorescence (Fig. 2A). Furthermore, the mCherry-positive EC exhibited mVenus fluorescence immediately after losing the red fluorescence, and then underwent cytokinesis (Fig. 2B). Time-lapse imaging analyses showed mVenus fluorescence at 278 ± 76 min ($n=6$) and 69 ± 44 min ($n=27$) before and after cell division, respectively. However, most of the mCherry-positive cells continued to exhibit mCherry fluorescence in the EC-zFucci embryos. Since mC-zCdt marks the cells not only in the G1 phase but also in the G0 phase of the cell cycle, these findings suggest that most of the mCherry-positive ECs had left the cell cycle. We further examined the effects of HU and APH, DNA replication inhibitors that induce S phase arrest (Carr, 2002; Ikegami et al., 1978), on the expression of mV-

Fig. 3. Cell-cycle progression of ECs during ISV formation. (A, B) Time-lapse confocal imaging of ISV sprouting from the dorsal aorta (DA) in the trunk region of a *Tg(flk1:mV-zGem);(flk1:NLS-mC)* fish embryo. (A) ISVs used for imaging analyses. An ISV of the boxed region is presented schematically. (B) 3D-rendered confocal 3D image of the embryo at 24.5 hpf (left upper) and its subsequent time-lapse images at the elapsed time (hr:min) indicated at the bottom (mVenus [green] and mCherry [red]). Note that an EC in the S/G2/M phase sprouts from the DA (arrows in 0:00 and 1:50), divides during dorsal migration (arrows in 3:10, 3:50, 4:20), leaves the M-phase (arrows in 5:10 and 6:40), and further migrates dorsally (arrow in 9:00) to form an ISV. (C) Percentages of mV-zGem-negative (−) and mV-zGem-positive (+) ECs involved only in forming ISV by sprouting from the DA. Data are shown as means ± s.d. ($n=5$). (D) Types of ECs that divide during ISV formation. Cell division was defined by the division of mV-zGem-positive ECs. The numbers of ISVs showing tip cell division (Tip), stalk cell division (Stalk) or division of both tip and stalk cells (Tip/Stalk) or showing no cell division (None) were divided by the total number of ISVs observed ($n=34$). (E) Quantification of the number of EC divisions during ISV formation. The numbers of ISVs showing no cell division, one, two, or three rounds of cell division divided by the total numbers of ISVs observed ($n=34$). (F) A model of cell-cycle regulation of ECs during ISV formation. (G) 3D-rendered confocal 3D images of the trunk regions of *Tg(flk1:mV-zGem);(flk1:NLS-mC)* embryos injected with control MO (upper panel) or *dll4* MO (lower panel) at 48 hpf. Upper, merged images (mVenus [green] and mCherry [red]) of control morphants; lower, those of *dll4* morphants. (H, I) The number of mV-zGem-positive cells (H) and the total number of ECs (I) within the five ISVs. Data are shown as means ± s.d. ($n=11$). (J) 3D-rendered confocal images of the trunk regions of 32 hpf *Tg(fli1:Myr-mC);(flk1:NLS-Eos)* embryos treated from 20 hpf with DMSO (left column) or HU/APH (right column). Upper, Eos images; lower, the merged images of Eos and mCherry. Scale bars, 100 μm. (K) The numbers of ECs in the posterior cardinal vein (PCV), DA and ISV/dorsal longitudinal anastomotic vessel (DLAV) within the five ISVs as observed in J were counted, and shown as means ± s.d. (DMSO [$n=9$], HU/APH [$n=11$]). ISV, intersegmental vessel; DA, dorsal aorta; DLAV, dorsal longitudinal anastomotic vessels. $^{**}p < 0.01$, $^{***}p < 0.001$ (C, H, I, K). n.s., no significance.

zGem in ECs (Fig. 2C, D). In the *Tg(flk1:mV-zGem);(fli1:Myr-mC)* embryos treated with HU and APH (HU/APH), mVenus fluorescence in ECs persisted for at least 10 h after starting the observation, whereas most of the mVenus-positive ECs had lost fluorescence by 6 h in the DMSO-treated embryos (Fig. 2D). Accordingly, the HU/APH-treated embryos exhibited increased numbers of mVenus-positive ECs (Fig. 2C), although the total number of ECs was decreased by HU/APH treatment, as described

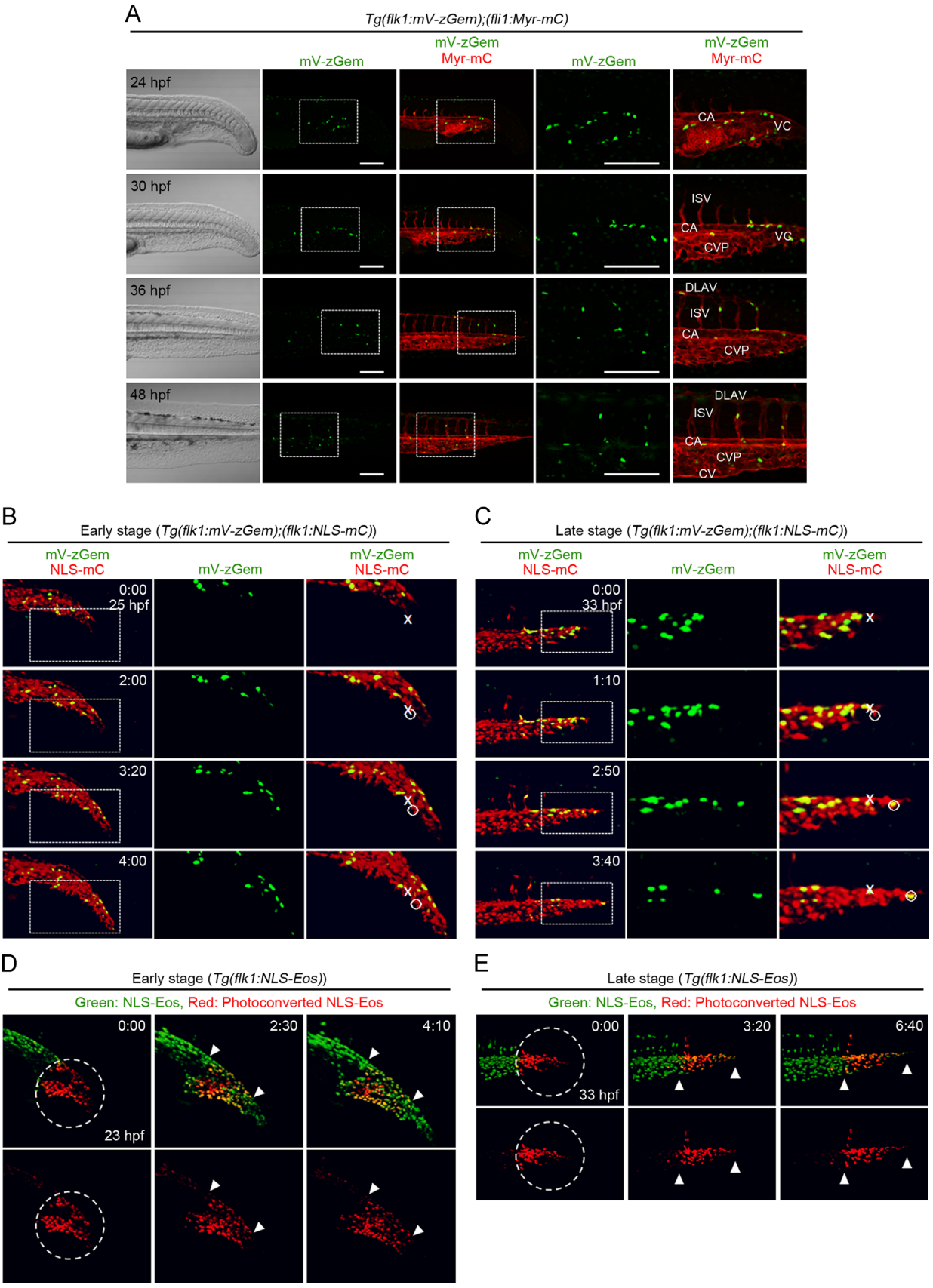

below. Collectively, these results indicate that the EC-zFucci fish line allows us to precisely visualize the cell-cycle progression of ECs in living animals.

Cell-cycle progression of ECs during intersegmental vessel formation

The development of ISVs in the zebrafish provides an excellent model system for the study of sprouting angiogenesis in vivo (Blum et al., 2008; Isogai et al., 2003; Lawson and Weinstein, 2002). During ISV formation, ECs sprout from the dorsal aorta (DA) and migrate along the somite boundary toward the dorsolateral roof of the neural tube. The EC located at the leading edge of each sprout is called the tip cell, and is followed by a few stalk cells. To investigate cell-cycle control in sprouting angiogenesis, we observed S/G2/M phase ECs during ISV formation by performing time-lapse imaging of *Tg(flk1:mV-zGem);(flk1:NLS-mC)* embryos in which NLS-tagged mCherry was expressed in the nuclei of ECs (Fig. 3A, B and Supplemental Movie 1). Approximately 80% of ECs that sprouted from the DA were found in the S/G2/M phase of the cell cycle (Fig. 3B, C). After sprouting from the DA, the cells in the S/G2/M phase became tip cells, migrated dorsally, and underwent cell division between horizontal myosepta, giving rise to both tip and stalk cells which immediately left the M-phase (Fig. 3B). The tip cell further migrated dorsally to form an ISV. Careful analysis of the time-lapse imaging results revealed that about 60% of tip cells divided during ISV formation (Fig. 3D). In addition, only one round of cell division occurred to form one ISV in approximately 70% of cases (Fig. 3E). These results show that ECs progressing through the cell cycle sprout from the DA, then undergo one round of cell division during dorsal migration and form ISVs (Fig. 3F).

Supplementary material related to this article can be found online at http://dx.doi.org/10.1016/j.ydbio.2014.06.015.

Delta-like 4 (Dll4)/Notch signal is known to regulate angiogenesis by restricting the angiogenic behavior of ECs (Bentley et al., 2008; Hellstrom et al., 2007; Leslie et al., 2007; Lobov et al., 2007; Siekmann and Lawson, 2007; Suchting et al., 2007). Indeed, impaired Dll4/Notch signaling in zebrafish results in hyperbranching of ISVs and an increased number of ECs in these ISVs (Leslie et al., 2007; Siekmann and Lawson, 2007). Thus, to further evaluate the applicability of the EC-zFucci fish line, we examined the effect of inhibiting Dll4/Notch signaling on the cell-cycle state of ECs by injecting a MO targeting *dll4* into *Tg(flk1:mV-zGem);(flk1:NLS-mC)* embryos. The number of S/G2/M phase ECs in ISVs was significantly increased by knocking down *dll4* (Fig. 3G,H). Although the total number of ECs in these ISVs was also increased in *dll4* morphants, the proportion of S/G2/M phase ECs to the total number of ECs was higher in Dll4-depleted embryos than in control embryos (control embryos, 161%; dll4 morphants, 226%) (Fig. 3H,I). These findings indicate that Dll4/Notch signaling regulates angiogenesis by restricting the cell-cycle progression of ECs. In addition, it has been shown that cyclin dependent kinase inhibitor 1b (Cdkn1b) suppresses angiogenesis by blocking the cell-cycle progression of ECs (Nicoli et al., 2012). Consistently, the depletion of *cdkn1b* significantly increased the number of S/G2/M phase ECs in ISVs (Supplemental Fig. S1). Thus, our findings further support the usefulness of the EC-zFucci fish line for studying EC proliferation in vivo.

Role of EC proliferation in ISV formation

The presence of proliferating ECs in ISVs suggests EC proliferation to be required for ISV formation. To address this hypothesis, we investigated the effect of inhibiting EC proliferation on the formation of ISVs. The *Tg(fli1:Myr-mC);(flk1:NLS-Eos)* embryos, in which the nuclei of the ECs had been labeled with Eos fluorescence, were treated with HU/APH from 20 hpf and analyzed at 32 hpf. Unexpectedly, basic framework structures of trunk vessels, consisting of ISVs, dorsal longitudinal anastomotic vessels (DLAVs), the DA and the posterior cardinal vein (PCV), formed in the embryos treated with HU/APH (Fig. 3J). Consistently, time-lapse imaging analysis of HU/APH-treated *Tg(fli1:Myr-mC);(flk1:NLS-Eos)* embryos revealed that the ECs sprouted from the DA, migrated dorsally and formed ISVs even in the presence of HU/APH (Supplemental Movie 2). These results indicate that migration of ECs from the DA can compensate for a lack of EC proliferation during ISV development. However, the numbers of ECs in these ISVs, DLAVs and the DA, but not in the PCV, were significantly decreased by HU/APH treatment (Fig. 3K). Therefore, EC proliferation appears to be indispensable for the formation of functionally mature ISVs.

Supplementary material related to this article can be found online at http://dx.doi.org/10.1016/j.ydbio.2014.06.015.

Cell-cycle progression of ECs during caudal vessel formation

In zebrafish, the body axis continues to extend after gastrulation as a tail forms at the posterior end of the embryo (Kanki and Ho, 1997). Concomitantly, the axial vessels elongate posteriorly, giving rise to caudal vessels (Isogai et al., 2001) (Fig. 4A). However, the mechanism underlying caudal vessel formation remains largely unknown. To explore this question, we investigated the cell-cycle state of ECs during caudal vessel formation. In the zebrafish embryo at 24 hpf, vascular cord structures formed at the posterior end of the axial vessels and contained many S/G2/M phase ECs (Fig. 4A). At 30 and 36 hpf, the ECs in the S/G2/M phase were mainly present in the vascular cord, caudal artery (CA) and ISVs at the growing edge of the caudal vessels (Fig. 4A). At 48 hpf, the ECs progressing through the cell cycle were observed to become localized mainly in the ISVs and caudal vein plexus (CVP) of the caudal vessels (Fig. 4A). These results suggest that EC proliferation may contribute to the outgrowth of caudal vessels.

To assess this possibility, we performed a time-lapse imaging study of *Tg(flk1:mV-zGem);(flk1:NLS-mC)* embryos during caudal vessel formation. At 25–29 hpf, ECs in the S/G2/M phase were located at the vascular cords, as shown in Fig. 4A, and proliferated actively (Fig. 4B and Supplemental Movie 3). Interestingly, however, NLS-mCherry-positive cells emerged just posterior to the growing edges of caudal vessels and coalesced with the preexisting vascular

Fig. 4. Cell-cycle progression of ECs during caudal vessel formation. (A) 3D-rendered confocal images of the caudal vessels of *Tg(flk1:mV-zGem);(fli1:Myr-mC)* embryos at 24, 30, 36 and 48 hpf as indicated in the first column from the left. Bright field images (left) and fluorescence images (as indicated at the top). The boxed areas of the second and the third columns are enlarged in the fourth and fifth columns, respectively. CA, caudal vessel; VC, vascular cord; ISV, intersegmental vessel; CVP, caudal vein plexus; DLAV, dorsal longitudinal anastomotic vessels. Scale bars, 100 μm. (B) Time-lapse confocal imaging of caudal vessel formation in the early stage (from 25 to 29 hpf) in the *Tg(flk1:mV-zGem);(flk1:NLS-mC)* embryos. The confocal 3D image of the embryo at 25 hpf (top) and subsequent time-lapse images (from second to fourth rows) as indicated by the elapsed time (hr:min) at the top right. Left, merged (mVenus and mCherry); center, enlarged mVenus images of the boxed region of the left panel; right, enlarged merged image of the boxed region of the left panel. The cell movement of the posterior-most cell at the beginning (crosses) and at the end (circles) during time-lapse imaging, as analyzed employing a cell tracking application. (C) *Tg(flk1:mV-zGem);(flk1:NLS-mC)* embryos in the late stage (from 33–37 hpf) were similarly time-lapse imaged and analyzed as in B. Note that NLS-mCherry-positive cells merge just posterior to the growing edges of caudal vessels in the early stage, but not in the late stage, of caudal vessel formation. (D) Time-lapse confocal imaging of caudal vessel formation at the early stage (from 23 to 27 hpf) in the *Tg(flk1:NLS-Eos)* embryos. Confocal 3D images (at 23 hpf) and subsequent time-lapse images of photoconverted NLS-Eos (red)-marked ECs (encircled) from original NLS-Eos (green)-marked cells by laser irradiation at 23 hpf. Elapsed time (hr:min). Upper, merged images of Eos (green) and photoconverted Eos (red); lower, photoconverted Eos (red) images. Arrowheads indicate the anteriormost and posteriormost of the photoconverted cells. (E) *Tg(flk1:NLS-Eos)* embryos in the late stage (from 33 to 40 hpf) were time-lapse imaged and analyzed as in D.

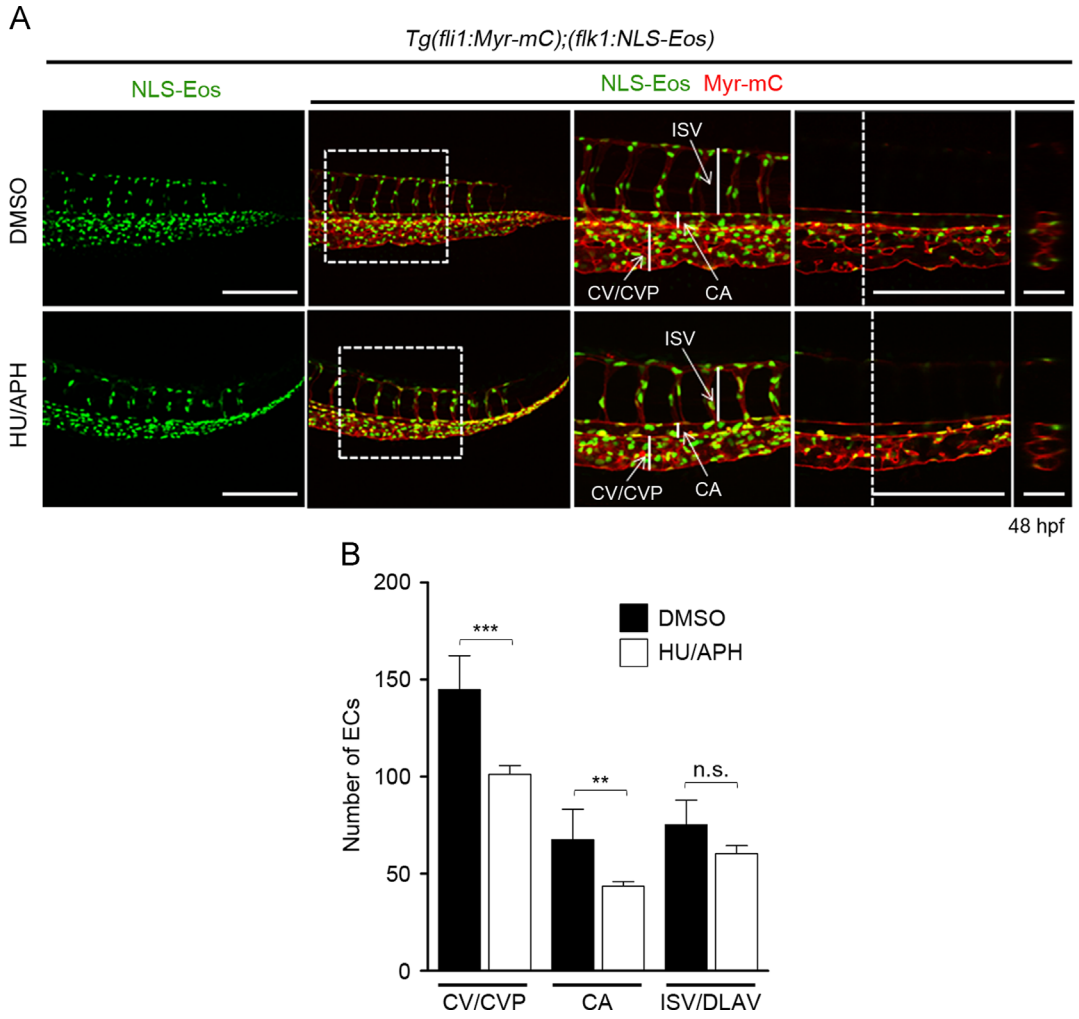

Fig. 5. Effect of inhibiting EC proliferation on caudal vessel formation. (A) 3D-rendered confocal images of the caudal regions of 48 hpf *Tg(fli1:Myr-mC);(flk1:NLS-Eos)* embryos treated from 24 hpf with DMSO (upper) or HU/APH (lower). Left column, Eos images; from the second to fifth columns, the merged images of Eos (green) and mCherry (red). The boxed areas in the second column and the corresponding single scan confocal images are enlarged in the third and fourth columns, respectively. The cross-sectional single plane images of the areas indicated by dotted lines on the fourth column are also shown in the fifth column. ISV, intersegmental vessel; CA, caudal artery; CV, caudal vein; CVP, caudal vein plexus. Scale bars, 100 μm (first and fourth columns) and 50 μm (fifth column). (B) The numbers of ECs in the CV/ CVP, CA and ISV/ DLAV within the five ISVs, as observed in A, were counted and shown as means ± s.d. (DMSO [$n=10$], HU/APH [$n=12$]). $^{**}p<0.01$, $^{***}p<0.001$. n.s., no significance.

cords (Fig. 4B and Supplemental Movie 3). In clear contrast, we detected no emergence of NLS-mCherry-positive cells in the caudal region at 33–36 hpf (Fig. 4C and Supplemental Movie 4). Instead, the ECs in the S/G2/M phase at the growing edges of caudal vessels proliferated actively and migrated posteriorly (Fig. 4C and Supplemental Movie 4). These results suggest that development and proliferation of angioblasts, namely vasculogenesis, both occur in the early stage of caudal vessel formation, while the ECs located at the growing edge proliferate and migrate in the late stage.

Supplementary material related to this article can be found online at http://dx.doi.org/10.1016/j.ydbio.2014.06.015.

To further confirm that vasculogenesis occurs during caudal vessel formation, we performed a time-lapse imaging study of *Tg (flk1:NLS-Eos)* embryos in which a photoconvertible fluorescence protein (NLS-Eos) was expressed in the nuclei of ECs. We photoconverted NLS-Eos-expressing ECs in the growing edges of caudal vessels at 23 hpf, and conducted time-lapse imaging for 4 h. Green fluorescence-positive cells appeared in the region just posterior to the photoconverted red fluorescence-marked cells (Fig. 4D and Supplemental Movie 5). We also marked the ECs in the posterior ends of caudal vessels at 33 hpf by photoconverting the NLS-Eos proteins. In clear contrast to embryos in the earlier stage, we detected no emergence of green fluorescence-positive cells. Instead, photoconverted red fluorescence-marked ECs migrated posteriorly, thereby leading to extension of caudal vessels (Fig. 4E and Supplemental Movie 6). Collectively, these findings indicate that caudal vessel development depends on the early stage on vasculogenesis that involves differentiation and proliferation of angioblasts, while proliferation and migration of ECs contribute to the posterior elongation of caudal vessels in the late stage.

Supplementary material related to this article can be found online at http://dx.doi.org/10.1016/j.ydbio.2014.06.015.

Role of EC proliferation in caudal vessel formation

To investigate the requirement of EC proliferation for caudal vessel formation, we treated the 24 hpf *Tg(fli1:Myr-mC);(flk1:NLS-Eos)* embryos with either DMSO or HU/APH for 24 h, and analyzed their caudal vessel structures at 48 hpf. In the caudal regions of DMSO-treated embryos, the CA formed at the midline, while the caudal vein (CV) and CVP were established at the ventral side of the CA (Fig. 5A). The ISVs and DLAVs also formed at the dorsal side. As in the DMSO-treated embryos, basic framework structures of caudal vessels developed in the HU/APH-treated embryos (Fig. 5A). Indeed, the axial vessels comprising the CA, CV and CVP had vascular lumens regardless of whether the embryos had been

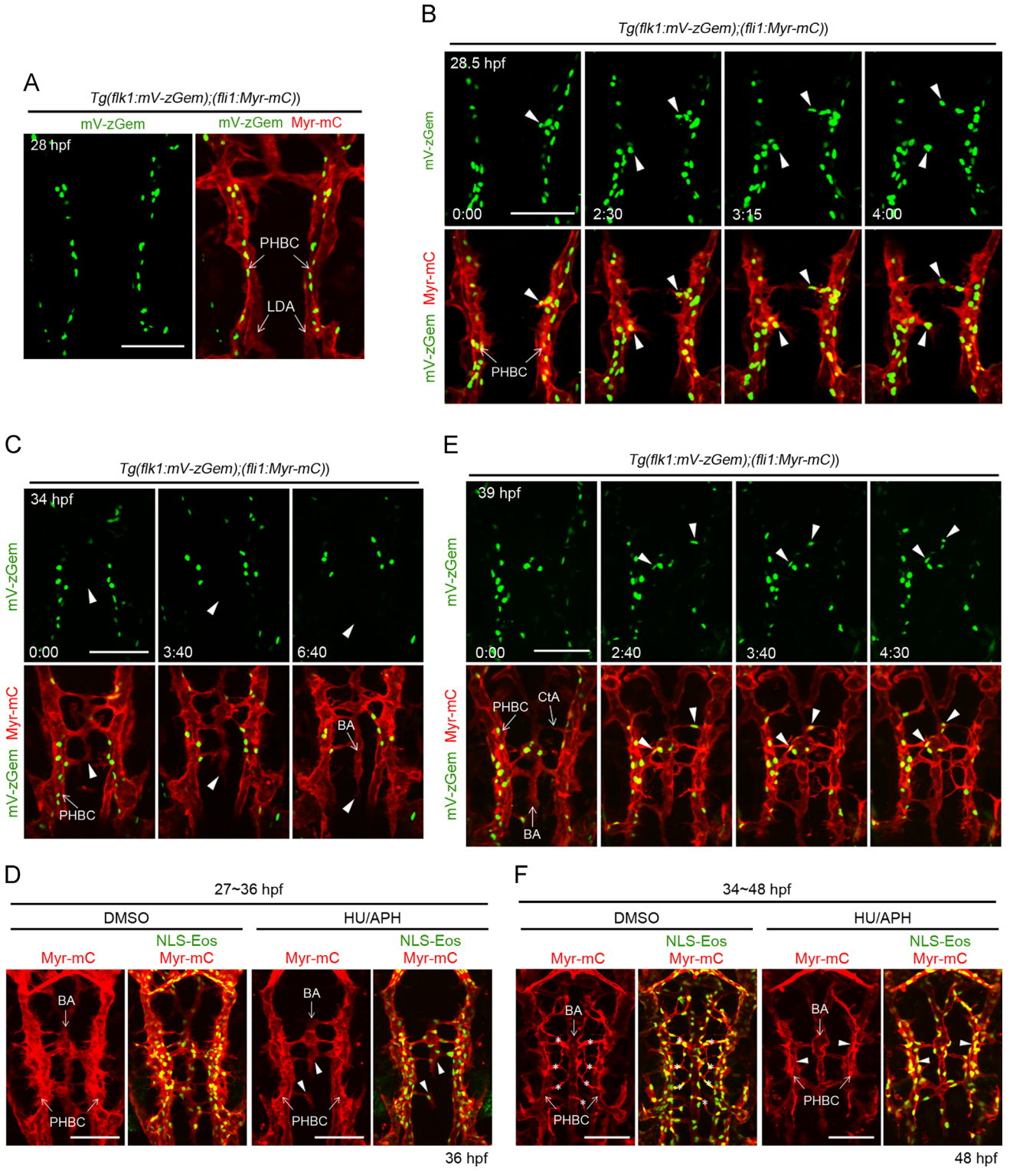

Fig. 6. Cell-cycle progression of ECs during formation of hindbrain vasculature. (A) 3D-rendered confocal images of the hindbrain vasculature in *Tg(flk1:mV-zGem);(fli1:Myr-mC)* embryos at 28 hpf. Left, mVenus image; right, the merged image of mVenus (green) and mCherry. All confocal images in this figure are dorsal views and displayed as anterior to the top. (B, C) 3D-rendered confocal fluorescence image of the hindbrain vasculature in *Tg(flk1:mV-zGem);(fli1:Myr-mC)* embryos at 28.5 hpf (B) or 34 hpf (C) and the corresponding subsequent time-lapse images at the elapsed time (h:min) indicated at the bottom of the upper panel. Upper, mVenus image; lower, the merged image of mVenus (green) and mCherry. Arrowheads indicate mVenus-positive ECs that sprout from the primordial hindbrain channels (PHBCs) (B) and the ECs that caudally migrate to form the basilar artery (BA) (C). (D) Confocal fluorescence image of the hindbrain vasculature in 36 hpf *Tg(fli1:Myr-mC);(flk1:NLS-Eos)* embryos treated from 27 hpf with DMSO (left) or HU/APH (right). mCherry and the merged images of mCherry (red) and Eos (green) are shown as indicated at the top. Arrowheads indicate defective formation of the BA. (E) Confocal fluorescence images of the hindbrain vasculature in *Tg(flk1:mV-zGem);(fli1:Myr-mC)* embryos at 39 hpf and the corresponding subsequent time-lapse images at the elapsed time (h:min) indicated at the bottom of the upper panel are shown, as in B. Arrowheads indicate mVenus-positive ECs that sprout from PHBCs to form the CtAs. (F) Confocal fluorescence images of the hindbrain vasculature in 48 hpf *Tg(fli1:Myr-mC);(flk1:NLS-Eos)* embryos treated from 34 hpf with DMSO (left) or HU/APH (right) are shown, as in D. Asterisks and arrowheads indicate CtAs and ECs failing to sprout from PHBCs to form the CtAs, respectively. PHBC, primordial hindbrain channels; LDA, lateral dorsal aorta; BA, basilar artery; CtA, central artery. Scale bars, 100 μm (A–F).

treated with DMSO or HU/APH (Fig. 5A). These findings show that EC proliferation is not essential for the formation of the basic framework structures of caudal vessels. However, the numbers of ECs in the CA, CV and CVP were significantly decreased by HU/APH treatment (Fig. 5B). Consistently, the distance from the most dorsal wall of the CA to the most ventral wall of the CV was shorter in the HU/APH-treated than in the DMSO-treated embryos (Fig. 5A). Therefore, these results suggest that EC proliferation may be required for full functional maturation of the caudal vasculature.

Cell-cycle progression of ECs during formation of hindbrain vasculature

The cranial vasculature is essential for maintaining the central nervous system, since it delivers oxygen and nutrients to the entire brain (Rolfe and Brown, 1997). Impairment of cranial vessel functions leads to cerebrovascular diseases such as stroke and intracranial hemorrhage (Segura et al., 2009). Thus, we decided to investigate the cell-cycle progression of ECs during cranial vessel

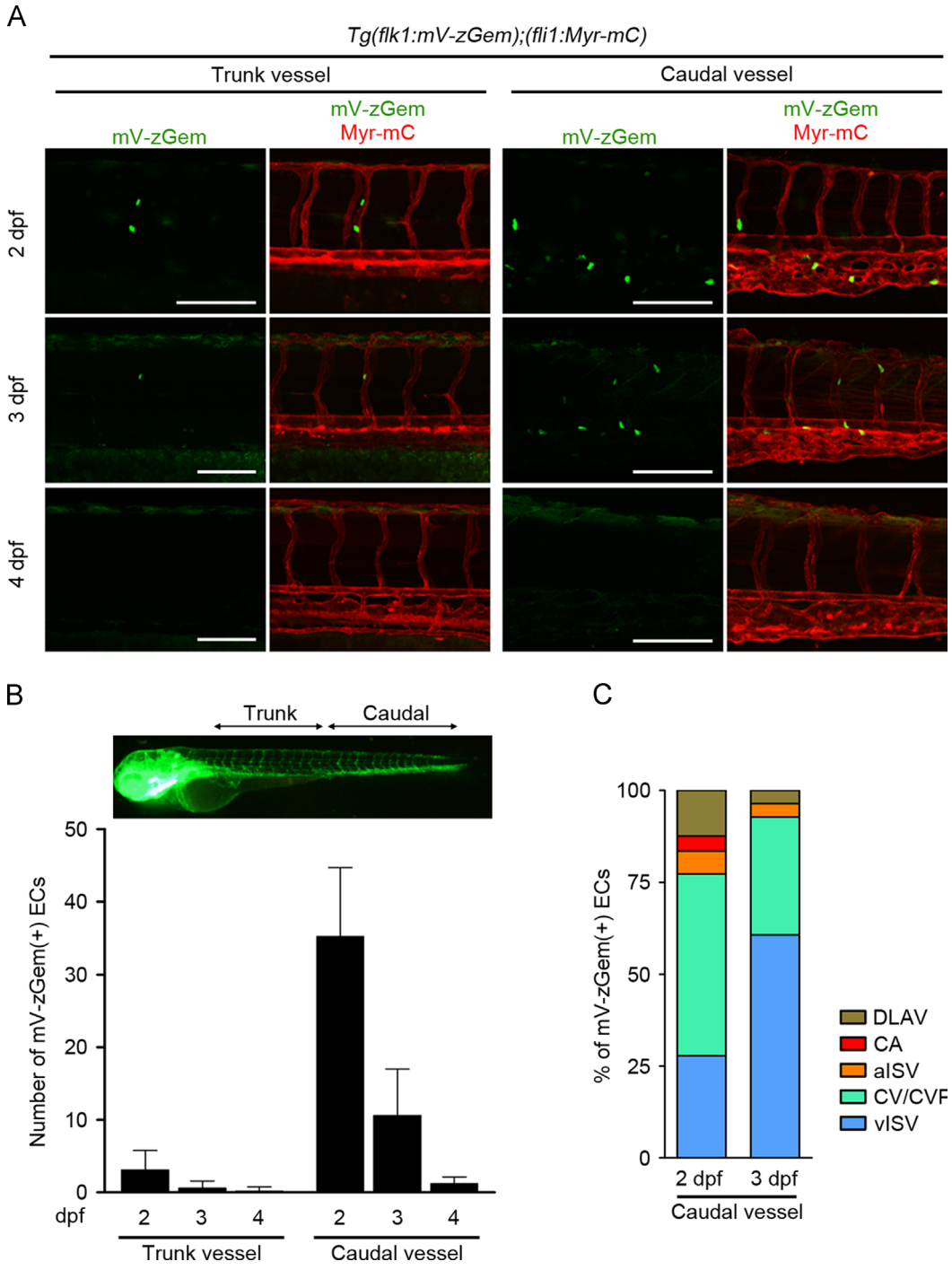

Fig. 7. Cell-cycle progression of ECs during the late stage of vascular development. (A) 3D-rendered confocal images of the trunk (left) and caudal (right) vasculature in the *Tg (flk1:mV-zGem);(fli1:Myr-mC)* embryos at 2, 3 and 4 dpf as indicated at the left. Left, mVenus image; right, the merged image of mVenus (green) and mCherry (red). Scale bars, 100 μm. (B) The numbers of mVenus-positive ECs in the trunk and caudal vasculature at 2, 3 and 4 dpf, as observed in A, were counted and shown as means ± s.d. (2 dpf [$n=16$], 3 dpf [$n=14$], 4 dpf [$n=13$]). (C) The numbers of mVenus-positive ECs in the DLAV, CA, arterial ISV (aISV), CV/CVP and venous ISV (vISV) of the caudal vasculature at 2 and 3 dpf were quantified, and then expressed as percentages of the total number (2 dpf [$n=97$], 3 dpf [$n=28$]).

formation. We focused on development of the hindbrain vasculature which is comprised mainly of two primordial hindbrain channels (PHBCs), the midline basilar artery (BA) and several central arteries (CtAs), since this has been analyzed in detail in studies focusing on how the hindbrain vasculature is formed, how ECs assemble, and how EC patterns are involved in vessel formation (Fujita et al., 2011; Isogai et al., 2001; Ulrich et al., 2011). Briefly, at the beginning of hindbrain vascular development, a pair of PHBCs forms on both sides of the ventral-lateral hindbrain by 22–24 hpf. At 28 hpf, ECs sprout from the medial walls of these PHBCs, migrate medially and form the precursor of the BA, a major artery in the hindbrain, at the ventral midline. Then, the ECs in the BA precursor align longitudinally and further migrate caudally to form the BA. Once assembly of the BA is complete, connections between the PHBCs and the BAs disappear. In addition to the BA, ECs sprout from the dorsal surfaces of the PHBCs and form the CtAs. The CtA sprouts first grow dorsally through the hindbrain at approximately 32 hpf, then turn ventrally and connect to the BA around 40–48 hpf, making vessel connections between the PHBCs and the BA.

First, we analyzed the cell-cycle state of ECs during BA formation by using *Tg(flk1:mV-zGem);(fli1:Myr-mC)* embryos. At 28 hpf, the PHBCs contained many S/G2/M phase ECs (Fig. 6A), indicating active proliferation of these ECs in PHBCs. This observation is consistent with the previously reported results that the diameter of PHBCs and the number of ECs in these PHBCs both increase between 24 and 36 hpf (Ulrich et al., 2011). However, although some of the ECs that sprouted from PHBCs were found to be in the S/G2/M phase of the cell-cycle (Fig. 6B), most of the ECs left the cell cycle after reaching the midline and/or during their subsequent caudal migration (Fig. 6C). To investigate the contribution of EC proliferation to BA formation, we treated the *Tg(fli1:Myr-mC);(flk1:NLS-Eos)* embryos with either DMSO or HU/APH for 27–36 hpf. By 36 hpf, the BA had formed at the ventral midline in DMSO-treated embryos, whereas the HU/APH-treated embryos exhibited defective BA formation (Fig. 6D). These results suggest that the ECs in PHBCs proliferate actively to supply the ECs migrating toward the midline and needed to form the BA, although EC proliferation does not actually occur during BA formation.

We next analyzed the cell-cycle progression of ECs during the formation of CtAs. The PHBCs still contained ECs in the S/G2/M phase of the cell cycle at 39 hpf. Although a few S/G2/M phase ECs were observed in the developing CtAs, most of the ECs that sprouted from PHBCs to form the CtAs were mVenus-negative (Fig. 6E). These results suggest that CtA formation depends mainly on migration of ECs derived from PHBCs but also, partly, on EC proliferation. We further investigated whether EC proliferation is required for CtA formation by treating the *Tg(fli1:Myr-mC);(flk1:NLS-Eos)* embryos with HU/APH for 34–48 hpf. The sprouting of ECs from PHBCs was severely impaired by HU/APH treatment (Fig. 6F). Concomitantly, the HU/APH-treated embryos exhibited a defect in CtA formation (Fig. 6F). These results suggest that the ECs derived from PHBCs contribute to CtA formation. Thus, proliferation of ECs sprouted from PHBCs is required not only for BA formation but also for CtA formation.

Cell-cycle progression of ECs in the late stage of vascular development

Finally, we analyzed the cell-cycle state of ECs in the late stage of vascular development. At 2 days post-fertilization (dpf), the trunk vasculature contained several ECs in the S/G2/M phase (Fig. 7A, B). However, these cells left the cell cycle at 3 and 4 dpf (Fig. 7A, B). On the other hand, many ECs in the S/G2/M phase of the cell cycle were present in caudal vessels at 2 dpf (Fig. 7A, B). However, the number of S/G2/M phase ECs in these caudal vessels was decreased by approximately 30% at 3 dpf as compared to that at 2 dpf (Fig. 7B). Furthermore, only a few cells that progressed through the cell cycle were present in caudal vessels at 4 dpf (Fig. 7A, B). These results show that more EC proliferation occurs in caudal than in trunk vessels in the late stage of vascular development.

We further investigated where ECs proliferate within caudal vessels in the late stage of vascular development by identifying the mVenus-positive cells in our *Tg(flk1:mV-zGem);(Fli1:Myr-mC)* embryos. At 2 and 3 dpf, most of the ECs in the S/G2/M phase of the cell cycle were found in venous vessels comprising the CV, CVP and venous ISV, while only minor populations of ECs were mVenus-positive in arterial vessels. These findings suggest that venous ECs mainly proliferate in the late stage of vascular development, whereas arterial ECs become quiescent at this stage.

Discussion

In the present study, by generating the EC-zFucci zebrafish line, in which zFucci biosensors were specifically expressed in ECs, we succeeded in devising a novel imaging system which allows the cell-cycle progression of ECs to be visualized in living animals. We assessed whether the EC-zFucci Tg line precisely monitors the cell-cycle state of ECs by labeling S phase ECs with EdU, by performing time-lapse imaging analyses and by examining the effects of cell-cycle inhibitors. Furthermore, we were able to clearly show the advantage of using the EC-zFucci Tg line by analyzing the cell-cycle progression of ECs during the development of several vascular structures including ISVs, caudal vessels and hindbrain vessels, during both the early and the late stages of vascular development.

The cell-cycle of ECs is finely controlled during ISV formation. The development of ISV is a suitable model for studying sprouting angiogenesis (Blum et al., 2008; Isogai et al., 2003; Lawson and Weinstein, 2002). Therefore, we analyzed the cell-cycle state of ECs during ISV formation, and found that ECs progressing through the cell cycle sprout from the DA and undergo one round of cell division during dorsal migration to form ISVs. Dll4/Notch signal is one of the most important negative regulators of sprouting angiogenesis. Indeed, inhibition of Dll4/Notch signaling leads to hyper-proliferation of ECs during ISV formation (Leslie et al., 2007; Siekmann and Lawson, 2007). In addition, cdkn1b, a target of *miR-221*, has been shown to inhibit EC proliferation during ISV formation (Nicoli et al., 2012). Consistently, our analyses using the EC-zFucci Tg line revealed that knockdown of either *dll4* or *cdkn1b* promotes cell-cycle progression of ECs in ISVs. Thus, the EC-zFucci Tg line appears to be a useful system for studying regulation of the EC cycle in vivo.

Even without EC proliferation in ISVs, ECs migrating from the DA were able to form the basic framework of ISVs and DLAV, although proliferation might be required for these vessels to be fully functional. Unexpectedly, inhibition of EC proliferation with HU/APH treatment did not inhibit the formation of ISVs and DLAVs, although the numbers of ECs in these vessels were significantly reduced (Fig. 3J, K). However, although Nicoli et al. also examined the effect of HU/APH on ISV formation, they observed a significant decrease not only in EC number but also in ISV length in the HU/APH-treated embryos at 27 hpf (Nicoli et al., 2012). Since we analyzed the HU/APH-treated embryos at 32 hpf, it is reasonable to speculate that inhibiting EC proliferation delayed ISV formation, but did not completely prevent it. Consistently, our time-lapse imaging analyses showed no abrogation of the sprouting of ECs from the DA and subsequent dorsal migration in response to HU/APH treatment (Supplemental Movie 2). Thus, these results suggest that EC proliferation and migration may contribute to ISV and DLAV formation.

The early stage of caudal vessel formation involves development and proliferation of angioblasts. It has been well demonstrated that angioblasts arise within the lateral plate mesoderm, and migrate medially to form a vascular cord at the trunk midline, which gives rise to the DA and PCV (Jin et al., 2005a; Swift and Weinstein, 2009; Zhong et al., 2001). In this study, we found that angioblasts emerged in the ventral part of the tail independently of angioblast formation in the trunk region and contributed to the formation of caudal vessels. Consistently, mesodermal progenitor cells reportedly exist in the ventral tail bud and have the ability to differentiate into both endothelial and somite cell lineages (Martin and Kimelman, 2012). Collectively, these findings suggest that the angioblasts contributing to the development of the trunk and caudal vasculatures have distinct origins.

Increases in the number of ECs, via cell proliferation, are not required for the formation of basic framework structures of caudal vessels, although these increases do appear to be necessary for the formation of functionally mature caudal vessels. Active proliferation of angioblasts and ECs at the growing edges of caudal vessels suggests the involvement of EC proliferation in caudal vessel formation. However, the basic structures of caudal vessels, including ISVs, DLAVs, CA, CV and CVP, could still be established in HU/APH-treated embryos, despite the numbers of ECs in these caudal vessels being decreased. Therefore, our observations suggest angioblast development and migration to be involved in formation of the basic structures of caudal vessels, whereas EC proliferation contributes to the generation of fully-functional caudal vessels.

Formation of BA and CtAs in the hindbrain largely depends on the proliferation of ECs in PHBCs. The ECs sprouting from PHBCs migrate medially to form the BA and CtAs (Fujita et al., 2011; Ulrich et al., 2011). Previously, Ulrich et al. investigated the cellular mechanisms underlying BA and CtA formation, and revealed EC migration from PHBCs to be the primary mechanism of the formations of the BA and CtA, while EC proliferation plays a minor role in these processes (Ulrich et al., 2011). Our imaging analyses of the EC-zFucci Tg fish revealed PHBCs to contain a large number of ECs progressing through the cell cycle, while most of the sprouting ECs destined to form the BA and CtAs left the cell-cycle. Furthermore, inhibition of EC division resulted in defective formation of the BA and CtAs. Therefore, the ECs in PHBCs proliferate actively to supply the ECs that will ultimately form the BA and CtAs.

Vessel growth in the late stage of vascular development depends mainly on the proliferation of venous ECs. In the EC-zFucci fish embryos at 2 and 3 dpf, the ECs in the S/G2/M cell-cycle phases were mainly present in venous vessels of the caudal vasculature, whereas most of the ECs in the arterial vessels left the cell cycle, suggesting venous EC proliferation to play a role in the late stage of vascular development. It is important to ascertain whether mainly venous ECs also proliferate in the adult vasculature. However, unfortunately, mVenus/mCherry-double negative ECs were detected in the vasculature of adult EC-zFucci Tg fish (data not shown), showing that the cell-cycle state of ECs cannot be adequately visualized in the adult EC-zFucci Tg fish. Thus, we need to improve the EC-zFucci Tg fish line to analyze the cell-cycle progression of ECs in adult fish.

In the present study, we established EC-zFucci Tg zebrafish lines that allow the spatiotemporal pattern of cell-cycle dynamics of ECs to be visualized in vivo. To date, we have been able to visualize ECs undergoing mitosis by utilizing Tg reporter lines in which the nuclei of ECs were labeled by NLS-tagged fluorescence proteins. However, these Tg lines do not allow identification of the ECs in each phase of the cell cycle. Therefore, the EC-zFucci Tg line is more suitable than endothelial-specific nuclear Tg lines for analyzing the cell-cycle dynamics of ECs. In addition, the EC-zFucci Tg line can be used for FACS-based isolation of ECs according to their cell-cycle stage. Furthermore, the genes implicated in the regulation of EC proliferation during vascular development could be identified by crossing the EC-Fucci fish lines with various mutant fishes exhibiting defects in vascular development or by performing MO-mediated knock-down of candidate genes. Thus, the EC-Fucci transgenic zebrafish line is anticipated to be a useful tool for addressing unanswered questions about the significance of EC proliferation in vascular development.

Acknowledgments

We thank N. Lawson (University of Massachusetts Medical School, USA) for the plasmid encoding fli1 promoter, D.Y. Stainier (The University of California, San Francisco) for the plasmid encoding flk1 promoter, and K. Kawakami (National Institute of Genetics, Japan) for the Tol2 system. We are also grateful to K. Hiratomi, W. Koeda, M. Sone, E. Okamoto, Y. Shintani and T. Babazono for excellent technical assistance and K. Shioya for excellent fish care.

This work was supported in part by Grants-in-Aid for Scientific Research on Innovative Areas “Fluorescence Live imaging” (No. 22113009 to S.F.) and “Neuro-Vascular Wiring” (No. 22122003 to N.M.) from the Ministry of Education, Culture, Sports, Science, and Technology, Japan, and by grants from the Japan Society for the Promotion of Science (to S.F., N.M.); the Ministry of Health, Labour, and Welfare of Japan (to N.M.); the Core Research for Evolutional Science and Technology program of the Japan Science and Technology Agency (CREST, JST) (to N.M.); Takeda Science Foundation (to S.F., N.M.); the Naito Foundation (to S.F.); Mochida Memorial Foundation for Medical and Pharmaceutical Research (to S.F.); Japan Cardiovascular Research Foundation (to S.F.).

Appendix A. Supporting information

Supporting information associated with this article can be found in the online version at http://dx.doi.org/10.1016/j.ydbio.2014.06.015.

References

Akimoto, S., Mitsumata, M., Sasaguri, T., Yoshida, Y., 2000. Laminar shear stress inhibits vascular endothelial cell proliferation by inducing cyclin-dependent kinase inhibitor p21Sdi1/Cip1/Waf1. Circ. Res. 86, 185–190.

Ang, X.L., Harper, J.W., 2004. Interwoven ubiquitination oscillators and control of cell cycle transitions. Sci. STKE 2004, e31.

Ausprunk, D.H., Folkman, J., 1977. Migration and proliferation of endothelial cells in preformed and newly formed blood vessels during tumor angiogenesis. Microvasc. Res. 14, 53–65.

Bentley, K., Gerhardt, H., Bates, P.A., 2008. Agent-based simulation of notch-mediated tip cell selection in angiogenic sprout initialisation. J. Theor. Biol. 250, 25–36.

Blum, Y., Belting, H.G., Ellertsdottir, E., Herwig, L., Luders, F., Affolter, M., 2008. Complex cell rearrangements during intersegmental vessel sprouting and vessel fusion in the zebrafish embryo. Dev. Biol. 316, 312–322.

Carmeliet, P., 2000. Mechanisms of angiogenesis and arteriogenesis. Nat. Med. 6, 389–395.

Carr, A.M., 2002. DNA structure dependent checkpoints as regulators of DNA repair. DNA Repair 1, 983–994.

Cattoretti, G., Becker, M.H., Key, G., Duchrow, M., Schluter, C., Galle, J., Gerdes, J., 1992. Monoclonal antibodies against recombinant parts of the Ki-67 antigen (MIB 1 and MIB 3) detect proliferating cells in microwave-processed formalin-fixed paraffin sections. J. Pathol. 168, 357–363.

Favot, L., Keravis, T., Lugnier, C., 2004. Modulation of VEGF-induced endothelial cell cycle protein expression through cyclic AMP hydrolysis by PDE2 and PDE4. Thromb. Haemost. 92, 634–645.

Fujita, M., Cha, Y.R., Pham, V.N., Sakurai, A., Roman, B.L., Gutkind, J.S., Weinstein, B. M., 2011. Assembly and patterning of the vascular network of the vertebrate hindbrain. Development 138, 1705–1715.

Hellstrom, M., Phng, L.K., Hofmann, J.J., Wallgard, E., Coultas, L., Lindblom, P., Alva, J., Nilsson, A.K., Karlsson, L., Gaiano, N., Yoon, K., Rossant, J., Iruela-Arispe, M.L.,

Kalen, J.J., Gerhardt, H., Betsholtz, C., 2007. Dll4 signalling through Notch1 regulates formation of tip cells during angiogenesis. Nature 445, 776–780.
Hendzel, M.J., Wei, Y., Mancini, M.A., Van, H.A., Ranalli, T., Brinkley, B.R., Bazett-Jones, D.P., Allis, C.D., 1997. Mitosis-specific phosphorylation of histone H3 initiates primarily within pericentromeric heterochromatin during G2 and spreads in an ordered fashion coincident with mitotic chromosome condensation. Chromosoma 106, 348–360.
Herbert, S.P., Stainier, D.Y.R., 2011. Molecular control of endothelial cell behaviour during blood vessel morphogenesis. Nat. Rev. Mol. Cell Biol. 12, 551–564.
Ikegami, S., Taguchi, T., Ohashi, M., Oguro, M., Nagano, H., Mano, Y., 1978. Aphidicolin prevents mitotic cell division by interfering with the activity of DNA polymerase-alpha. Nature 275, 458–460.
Isogai, S., Horiguchi, M., Weinstein, B.M., 2001. The vascular anatomy of the developing zebrafish: an atlas of embryonic and early larval development. Dev. Biol. 230, 278–301.
Isogai, S., Lawson, N.D., Torrealday, S., Horiguchi, M., Weinstein, B.M., 2003. Angiogenic network formation in the developing vertebrate trunk. Development 130, 5281–5290.
Jin, S.W., Beis, D., Mitchell, T., Chen, J.N., Stainier, D.Y., 2005a. Cellular and molecular analyses of vascular tube and lumen formation in zebrafish. Development 132, 5199–5209.
Jin, S.W., Beis, D., Mitchell, T., Chen, J.N., Stainier, D.Y.R., 2005b. Cellular and molecular analyses of vascular tube and lumen formation in zebrafish. Development 132, 5199–5209.
Kanki, J.P., Ho, R.K., 1997. The development of the posterior body in zebrafish. Development 124, 881–893.
Kawakami, K., Takeda, H., Kawakami, N., Kobayashi, M., Matsuda, N., Mishina, M., 2004. A transposon-mediated gene trap approach identifies developmentally regulated genes in zebrafish. Dev. Cell 7, 133–144.
Kimmel, C.B., Ballard, W.W., Kimmel, S.R., Ullmann, B., Schilling, T.F., 1995. Stages of embryonic development of the zebrafish. Dev. Dyn. 203, 253–310.
Kimura, I., Honda, R., Okai, H., Okabe, M., 2000. Vascular endothelial growth factor promotes cell-cycle transition from G0 to G1 phase in subcultured endothelial cells of diabetic rat thoracic aorta. Jpn. J. Pharmacol. 83, 47–55.
Lawson, N.D., Weinstein, B.M., 2002. in vivo imaging of embryonic vascular development using transgenic zebrafish. Dev. Biol. 248, 307–318.
Leslie, J.D., Ariza-McNaughton, L., Bermange, A.L., McAdow, R., Johnson, S.L., Lewis, J., 2007. Endothelial signalling by the Notch ligand Delta-like 4 restricts angiogenesis. Development 134, 839–844.
Lobov, I.B., Renard, R.A., Papadopoulos, N., Gale, N.W., Thurston, G., Yancopoulos, G. D., Wiegand, S.J., 2007. Delta-like ligand 4 (Dll4) is induced by VEGF as a negative regulator of angiogenic sprouting. Proc. Natl. Acad. Sci. USA 104, 3219–3224.
Martin, B.L., Kimelman, D., 2012. Canonical Wnt signaling dynamically controls multiple stem cell fate decisions during vertebrate body formation. Dev. Cell 22, 223–232.
Nakayama, K.I., Nakayama, K., 2006. Ubiquitin ligases: cell-cycle control and cancer. Nat. Rev. Cancer 6, 369–381.
Nicoli, S., Knyphausen, C.P., Zhu, L.J., Lakshmanan, A., Lawson, N.D., 2012. miR-221 is required for endothelial tip cell behaviors during vascular development. Dev. Cell 22, 418–429.
Risau, W., 1997. Mechanisms of angiogenesis. Nature 386, 671–674.
Risau, W., Flamme, I., 1995. Vasculogenesis. Annu. Rev. Cell Dev. Biol. 11, 73–91.
Rolfe, D.F., Brown, G.C., 1997. Cellular energy utilization and molecular origin of standard metabolic rate in mammals. Physiol. Rev. 77, 731–758.
Roman, B.L., Pham, V.N., Lawson, N.D., Kulik, M., Childs, S., Lekven, A.C., Garrity, D. M., Moon, R.T., Fishman, M.C., Lechleider, R.J., Weinstein, B.M., 2002. Disruption of *acvrl1* increases endothelial cell number in zebrafish cranial vessels. Development 129, 3009–3019.
Sakaue-Sawano, A., Kurokawa, H., Morimura, T., Hanyu, A., Hama, H., Osawa, H., Kashiwagi, S., Fukami, K., Miyata, T., Miyoshi, H., Imamura, T., Ogawa, M., Masai, H., Miyawaki, A., 2008. Visualizing spatiotemporal dynamics of multicellular cell-cycle progression. Cell 132, 487–498.
Segura, I., De, S.F., Hohensinner, P.J., Ruiz de, A.C., Carmeliet, P., 2009. The neurovascular link in health and disease: an update. Trends Mol. Med. 15, 439–451.
Siekmann, A.F., Lawson, N.D., 2007. Notch signalling limits angiogenic cell behaviour in developing zebrafish arteries. Nature 445, 781–784.
Suchting, S., Freitas, C., le Noble, F., Benedito, R., Bréant, C., Duarte, A., Eichmann, A., 2007. The Notch ligand Delta-like 4 negatively regulates endothelial tip cell formation and vessel branching. Proc. Natl. Acad. Sci. USA 104, 3225–3230.
Sugiyama, M., Sakaue-Sawano, A., Iimura, T., Fukami, K., Kitaguchi, T., Kawakami, K., Okamoto, H., Higashijima, S.i., Miyawaki, A., 2009. Illuminating cell-cycle progression in the developing zebrafish embryo. Proc. Natl. Acad. Sci. USA 106, 20812–20817.
Swift, M.R., Weinstein, B.M., 2009. Arterial-venous specification during development. Circ. Res. 104, 576–588.
Ulrich, F., Ma, L.H., Baker, R.G., Torres-Vazquez, J., 2011. Neurovascular development in the embryonic zebrafish hindbrain. Dev. Biol. 357, 134–151.
Urasaki, A., Morvan, G., Kawakami, K., 2006. Functional dissection of the Tol2 transposable element identified the minimal cis-sequence and a highly repetitive sequence in the subterminal region essential for transposition. Genetics 174, 639–649.
Yu, C.C., Woods, A.L., Levison, D.A., 1992. The assessment of cellular proliferation by immunohistochemistry: a review of currently available methods and their applications. Histochem. J. 24, 121–131.
Zhang, L., Kendrick, C., Julich, D., Holley, S.A., 2008. Cell cycle progression is required for zebrafish somite morphogenesis but not segmentation clock function. Development 135, 2065–2070.
Zhong, T.P., Childs, S., Leu, J.P., Fishman, M.C., 2001. Gridlock signalling pathway fashions the first embryonic artery. Nature 414, 216–220.
Zhou, J., Lee, P.L., Tsai, C.S., Lee, C.I., Yang, T.L., Chuang, H.S., Lin, W.W., Lin, T.E., Lim, S.H., Wei, S.Y., Chen, Y.L., Chien, S., Chiu, J.J., 2012. Force-specific activation of Smad1/5 regulates vascular endothelial cell cycle progression in response to disturbed flow. Proc. Natl. Acad. Sci. USA 109, 7770–7775.